Simulation of Rotor-Foundation-Interaction on Tidal Current Turbines with Computational Fluid Dynamics

Matthias Arnold[#1], Frank Biskup[*2], Denis Matha[#3], Po Wen Cheng[#4]

[#]*Stuttgart Chair of Wind Energy (SWE),University Stuttgart*
Allmandring 5b, 70569 Stuttgart, Germany

[1]Arnold@ifb.uni-stuttgart.de

[3]Matha@ifb.uni-stuttgart.de

[4]Cheng@ifb.uni-stuttgart.de

[*]*Voith Ocean Current Technologies GmbH & Co. KG*
Alexanderstr. 11, 89522 Heidenheim, Germany

[2]Frank.Biskup@voith.com

Abstract **In this research the interaction of the rotor hydrodynamics with the foundation of a Tidal Energy Converter (TEC) are investigated. A detailed model of the turbine is built up and simulated with Computational Fluid Dynamics (CFD). The results of these simulations are used to compare the 4 load states of up- and downstream, below and above rated operation with respect to the rotor performance coefficients. The paper concludes with a comparison to results of simplified models and shows that the interaction can be simulated by an empirical approach.**

Keywords **Tidal Energy, Tidal Current Turbine, Hydrodynamics, Rotor, Computational Fluid Dynamics (CFD), Foundation, Rotor-Stator-Interaction, Vortex, Wake, Load Simulation**

I. Introduction

For visualizing a Tidal Energy Converter (TEC) there are 2 main components: the rotor and the foundation. They are both exposed to the flow and therefore significantly affect loads on the turbine. Through interaction both components also have an influence on each other. Therefore in this paper, the interaction of the rotor and foundation of a TEC is analysed with CFD methods and compared with the simplified Blade Element Momentum Method (BEM).

II. Methodology

The main results of this research are gathered by the analysis of transient CFD simulation as described below.

A. Tidal Current Turbine

During this research a TEC according to the dimensions and setup of the Voith HyTide 1000-13® 1MW Turbine, [12], has been used. This turbine is designed to produce an electrical power output of 1MW and will be installed for prototype testing at EMEC, [5], in 2013. The turbine is designed for maximum reliability under rough conditions. It therefore has no pitch, yaw and gearbox system.

The foundation consists of a tubular monopile and a rectangular transition piece to the turbine nacelle. This leads to a hub height of $h_{hub} = 15m$. The rotor is equipped with rotor blades of a tip diameter of $D_{tip} = 13m$. Based on the turbine concept the rotor is build bidirectional with a point-symmetric cross section optimized for maximum power production under acceptable loads. Details on thrust and power of the rotor blade in numerical and experimental investigations are given by [3].

A CAD image of the turbine setup and dimensions is shown in Fig. 1.

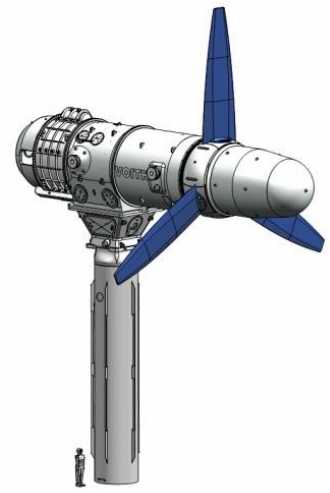

Fig. 1 Voith HyTide 1000-16® 1MW Tidal Current Turbine

B. Load States

To give a good representation of the points of operation a fatigue load state (FLS) and an ultimate load state (ULS) are defined. The fatigue load state represents the below rated operation in medium current speeds with $v_{FLS} = 2.2\,\frac{m}{s}$ at hub

height $h_{ref} = h_{hub} = 15m$ and optimal tip speed ratio $\lambda_{FLS} = \lambda_{Design}$.

The ultimate load state taken into account here occurs in above rated operation with an extreme flow velocity $v_{ULS} = 4\frac{m}{s}$ where the turbine speeds up to run away. This maximum or run away tip speed ratio is approximated to $\lambda_{ULS} = 2 \cdot \lambda_{Design}$ according to results from wind energy literature, [6].

The current shear is defined by Eq. 1 with a shear exponent $c_z = 0.19$ according to measurements of [7]. The water depth is $h_{msl} = 34.5m$ in a calm sea state and a plane ground level.

$$v(z) = v_{ref} \cdot \left(\frac{z}{h_{ref}}\right)^{c_z} \quad (1)$$

Due to the missing pitch and yaw mechanism for increased reliability and the change in flow direction during a tide cycle, the rotor operates under both, upstream and downstream configuration with respect to the foundation. For identification of effects of rotor stator interaction, 2 corresponding points of operation for below and above rated are added without foundation. The 6 points of operation simulated in this research are summarized in Tab. I.

TABLE I
SIMULATED LOAD STATES

Load State	Current $v\left[\frac{m}{s}\right]$	Orientation	Tip speed ratio λ	Indices
Ref below rated	2.2	No Tower	λ_{Design}	_below-ref
Ref above rated	4	No Tower	$2 \cdot \lambda_{Design}$	_above-ref
I	2.2	Upstream	λ_{Design}	_below-luv
II	4	Upstream	$2 \cdot \lambda_{Design}$	_above-luv
III	2.2	Downstream	λ_{Design}	_below-lee
IV	4	Downstream	$2 \cdot \lambda_{Design}$	_above-lee

C. CFD Model

The turbine has been simplified for generation of the mesh. In comparison to the CAD geometry shown in Fig. 1, the surface of the nacelle and foundation have been smoothed and all bolts, fastening points and flanges have been neglected. To take their effect into account, the surface is simulated with a numerical sand roughness according to a mean height of the neglected elements. The resulting simplified geometry is shown in Fig. 2.

The domain has been meshed in 4 grid sections as shown in Fig. 3. Each section consists of surface aligned structured hexahedron elements as shown in Fig. 4 with a total number of $8.59 \cdot 10^6$ elements for the full domain with 3 rotor blades and foundation.

The simulations in this research have been performed with the finite volume RANS CFD code Ansys CFX. The turbulence was modelled with the shear stress transport-turbulence model (SST) and all boundary layers are assumed to be fully turbulent. As shown by [1] and [8] by comparison to experimental data the SST model delivers good results for round trailing edge objects as investigated within this research. Based on the available computational resources the application of turbulence models of higher complexity as reynolds stress models (RSM) or detached eddy simulation (DES) was not feasible.

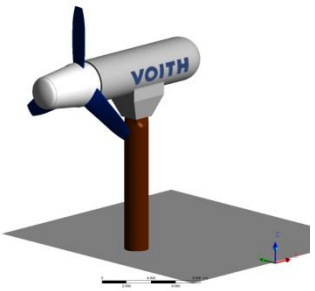

Fig. 2 simplified geometry for CFD analysis

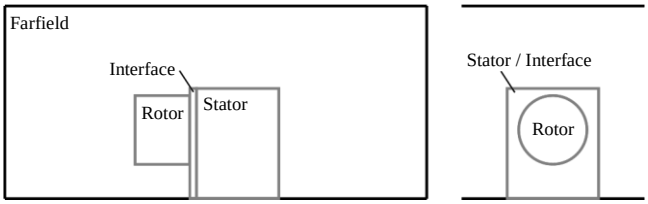

Fig. 3 grid structure with 4 sections

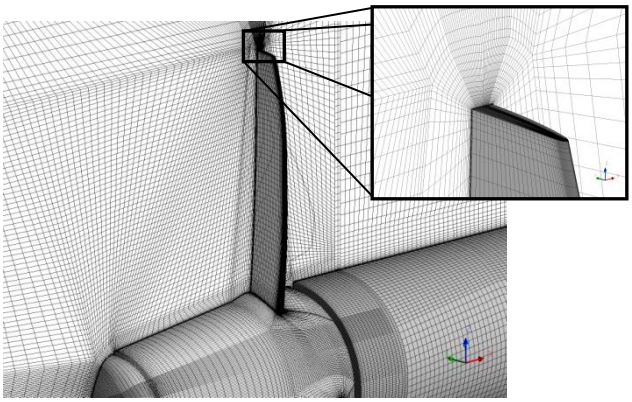

Fig. 4 structured grid on a rotor blade

The inflow was approximated as steady with 10% turbulent kinetic energy. Anyhow, this value is of less importance within this research. Due to the implementation of turbulence models in Ansys CFX this value decays rapidly, [4]. Therefore the value of turbulent kinetic energy is $\ll 1\%$ at the turbine location.

All simulations were performed with a transient rotation resolution of $\Delta\varphi = 6°$ over $3 - 5$ revolutions depending on tip speed ratio λ for convergence of the wake, followed by 2 revolutions with $\Delta\varphi = 3°$. Only the last revolution is then analysed in post processing.

III. RESULTS

Two types of results can be discerned. On one hand the qualitative results identifying vortex structures and differences between the load states, on the other hand the quantitative

results giving the effect of each vortex structure to the loads on the rotor.

A. Qualitative Analysis

In Fig. 5 the flow velocity in below rated operation for upstream and downstream direction of flow is compared in the foundation-nacelle-plane. In this plane 2 main wake structures can be identified. These are the rotor wake and the foundation wake. While the rotor wake is a more homogenous wake, in the foundation wake vortex shedding is present. The time averaged depth of the foundation wake is the same for upstream and downstream operation, but the momentaneous flow field shown in Fig. 5 differs, due to differences in the simulation and convergence procedure.

For upstream and downstream situations the rotor wake develops in nearly the same way. Both rotor wakes are bound on top position by a tip vortex, which can be identified for upstream condition at 5 locations and for downstream condition at 4 locations by a locally increased velocity in the analysis plane. This difference in dissipation of the tip vortex might be neglected due to the point, that the difference in grid resolution above the nacelle for $I_{below-luv}$ and in farfield for $III_{below-lee}$ causes increased numerical damping for $III_{below-lee}$.

A difference between $I_{below-luv}$ and $III_{below-lee}$ occurs for the tip vortex on the bottom position. For upstream operation, a tip vortex is shed and convects with the flow. After 1 rotation of the rotor it hits the foundation and the wake of the foundation is split into 2 sections in and out of the rotor wake. These are separated by a layer of increased flow velocity.

For downstream operation the rotor operates within the foundation wake and the angles of attack on the rotor blade are significantly reduced. Therefore no tip vortex is shed on the bottom position and also the depth of rotor wake is reduced for vertical down, $\varphi = 180°$, position of the rotor blade. This leads to an area of increased flow velocity in rotor wake for $III_{below-lee}$, which is mixed with the mean rotor wake within approx. 1D.

The same effects as reported for below rated operation are also present for above rated operation in load states $II_{above-luv}$ and $IV_{above-lee}$ as shown in Fig. 6. By direct comparison of below and above rated conditions it can be noticed, that the effects of Rotor-Foundation-Interaction reported above have a more intensive impact to the flow field.

Also it can be noticed, that there is a difference in flow for $I_{below-luv}$ compared to all other cases. Except for $I_{below-luv}$ the flow around the nacelle is homogenous with the expected boundary layer. For $I_{below-luv}$ the flow separates as shown in Fig. 7 at the transition piece between foundation and nacelle. This separation is then deformed by the rotor swirl around the nacelle. Due to not optimal operation and subsequent to the reduced torque coefficient this effect is not present for load state $II_{above-luv}$. This separation has only minor effect to the rotor hydrodynamics, but is of interest for near wake investigations.

By investigating the 3-dimensional flow around the nacelle, a horseshoe vortex starting from the stagnation point of the transition piece can be identified in Fig. 8. This horseshoe vortex moves along the nacelle at $\varphi \approx 90°$ and $\varphi \approx 270°$ at the sides of the nacelle. For $I_{below-luv}$ it cannot be observed due to the flow separation around the nacelle. For downstream operation the horseshoe vortex moves into the rotor plane and influences the rotor hydrodynamics, Fig. 9.

The last identified relevant effect is the 3-dimensional wake of the foundation for downstream operation. Due to the same dimensions in diameter of transition piece and nacelle, the inflow to the rotor forms a co-rotating and counter-rotating area. This rotating inflow increases respectively decreases the angle of attack at the rotor blades.

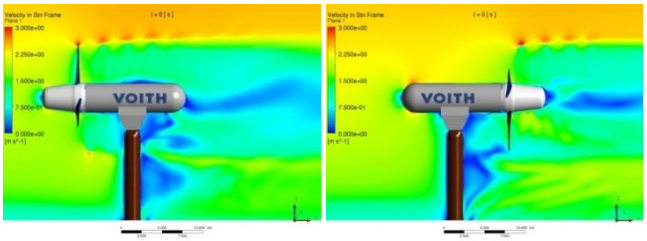

Fig. 5 comparison of load states $I_{below-luv}$ (left) and $III_{below-lee}$

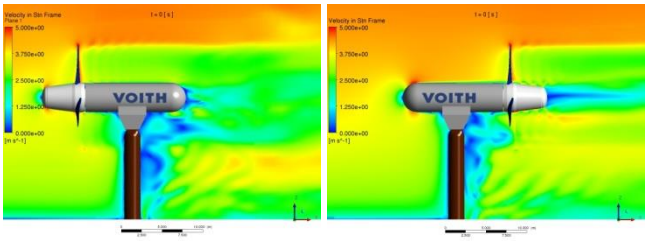

Fig. 6 comparison of load states $II_{above-luv}$ (left) and $IV_{above-lee}$

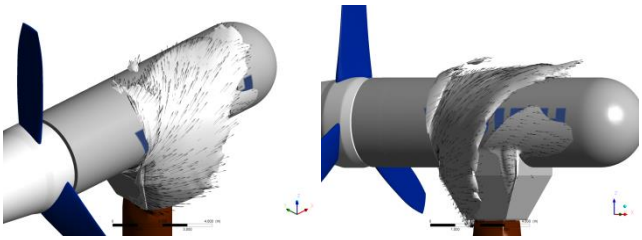

Fig. 7 flow separation at transition piece for load state $I_{below-luv}$

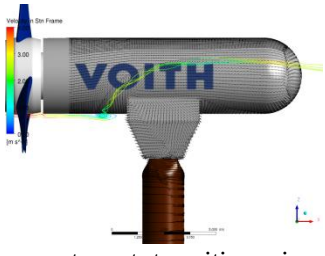

Fig. 8 horseshoe vortex at transition piece in load state $II_{above-luv}$

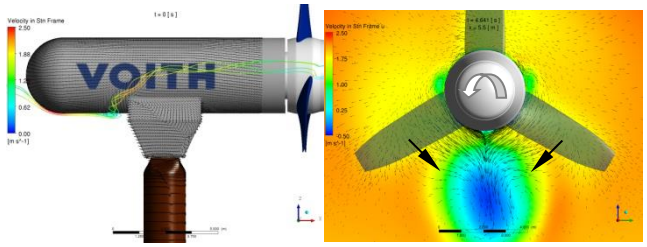

Fig. 9 horseshoe vortex at transition piece (left) and flow between foundation and rotor (right) in load state $III_{below-lee}$

B. Quantitative Analysis

To evaluate the above described effects of vortices to the rotor hydrodynamics, in Fig. 10 and Fig. 11, the thrust coefficient $c_{Th\ Blade}$ and power coefficient $c_{P\ Blade}$ of a single rotor blade is shown. Both values are given relative to the design values at λ_{Design} for better visualization denoted as $\bar{c}_{Th\ Blade}$ resp. $\bar{c}_{P\ Blade}$.

As can be seen for load states $I_{below-luv}$ and $II_{above-luv}$ compared to the reference values without foundation, the upstream tower shadow only amplifies the effect of free stream shear in inflow. No detailed effects of the vortices given above are in a noticeable range. Therefore a reduction of the effects to a simplified method can be done with an empirical method as supposed by [11] without limitations.

In difference to that the rotor in downstream operation in load states $III_{below-lee}$ and $IV_{above-lee}$ is significantly influenced by vortex structures. The most obvious effect results from the wake of the foundation itself. As described above the deceleration of flow is reduced for $\varphi = 180°$. This can be confirmed by the quantitative results, showing that the thrust coefficient of the rotor blade is reduced.

Besides this most significant effect, the influence of the horseshoe vortices can be identified as a reduction of the thrust and power coefficient over a short range at the position of the vortices. The position of the reduction in values at approx. $\varphi = \{70°, 250°\}$ does not fully correlate with the positions of the vortices. This phase shift occurs due to a finite blade chord length at hub and therefore a difference in blade position φ and the leading edge position φ_{lead} interacting with the vortices. Also a slight difference in position depending on the point of operation can be observed due to the changes in depth of rotor wake and generated rotor swirl.

A minor, but effect with a wider range can be observed for the co- and counter-rotating inflow to the rotor. Based on the subsequent changes in angle of attack, the thrust and power coefficient are increased for $\varphi < 180°$ and decreased for $\varphi > 180°$. This leads to a yawing torque around the foundation.

It can therefore be concluded, that there are multiple vortices with a relevant effect to the loads on the rotor blades. These effects need to be simulated as adequately as possible for fatigue and ultimate load case simulations.

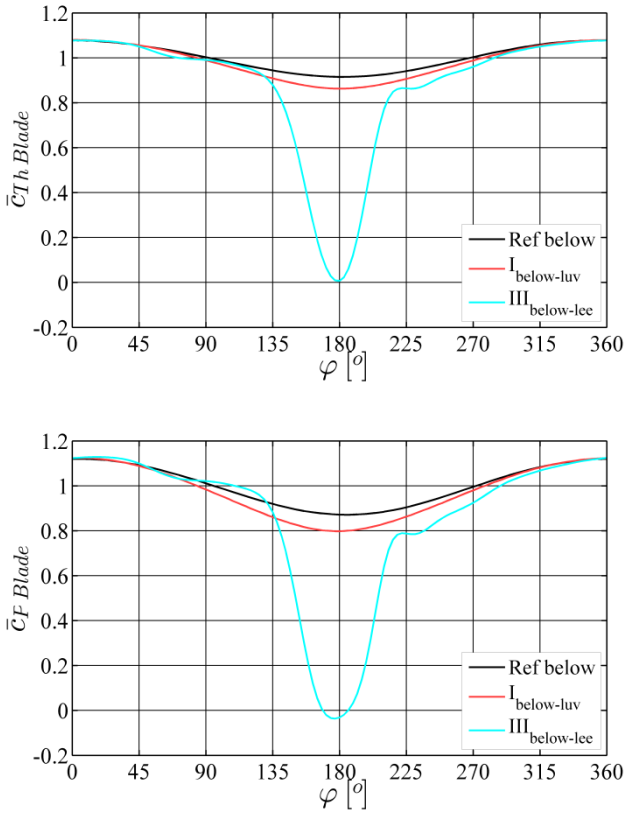

Fig. 10 relative thrust coefficient $\bar{c}_{Th\ Blade}$ (top) and power coefficient $\bar{c}_{P\ Blade}$ on rotor blade for operation below rated

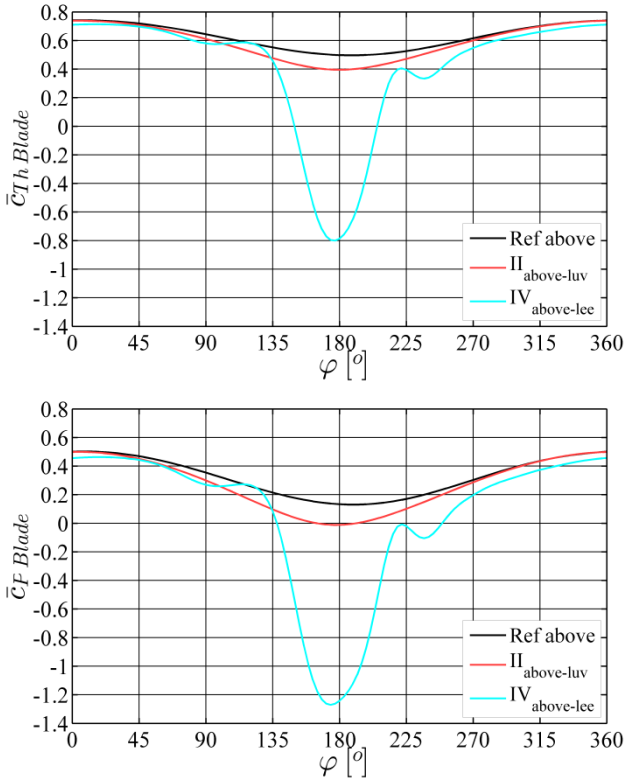

Fig. 11 relative thrust coefficient $\bar{c}_{Th\ Blade}$ (top) and power coefficient $\bar{c}_{P\ Blade}$ on rotor blade for operation above rated

IV. Simplified Models

For simulation of fatigue loads and ultimate load case operations it is not feasible to simulate these with CFD-methods due to high computational resources required. Therefore simplified models are used based on empirical and analytical approaches. The most common method for free rotors such as tidal or wind turbines is the Blade Element Momentum method (BEM). This is described in detail in [6].

In this research a state of the art implementation of BEM is used. The tower shadow for downstream operation is approximated by the empirical definition in Eq. 2, [11]. Within this empirical approximation, the constants e_{def} for the velocity deficit and W_{def} for the area of influence needs to be estimated for the given geometry either by measured or by simulated reference data. Within this work e_{def} and W_{def} are estimated based on the CFD results.

$$V(\vec{x},t) = \left(1 - e_{def} \cdot \cos^2\left(\frac{\pi \cdot y}{W_{def} \cdot D_T}\right)\right) \cdot V_0(\vec{x},t) \qquad (2)$$

As shown in Table II, two cases need to be distinguished. These are based on two different models within the implementation of the BEM. The Equilibrium Wake model (EQ) only takes instantaneous velocity and flow effects into account, while the Dynamic Inflow model (Dyn) takes also the history of flow conditions and transient effects in the flow into account, [9], [10].

With both models, the effect of tower wake can be simulated accurately as shown in Fig. 12 resp. Fig. 13 for the thrust coefficient in load state $III_{below-lee}$. By setting appropriate values for e_{def} and W_{def} the wake deficit fits the CFD results well. Obviously the effects of the single vortices cannot be present in the results of the simplified model.

Also a difference occurs for the top position of the rotor blade, $\varphi = \{0°, 360°\}$. This is a basic mismatch between CFD and BEM which needs to be adjusted via further empirical constants, e.g. tip and hub loss, as shown by [1] and is not further investigated in this work. Due to the Dynamic Inflow model taking transient effects into account, a phase shift in the results occur as can be seen in Fig. 12. This has been investigated by [9].

Besides the thrust coefficient $\bar{c}_{Th\,Blade}$ also the power coefficient $\bar{c}_{P\,Blade}$ matches with the above defined empirical model for above and below rated operation. Therefore it can be deducted that the simulation of the basic effects of Rotor-Foundation-Interaction can be done with simplified models, but for the detailed interaction CFD is still required.

TABLE II
TOWER WAKE PARAMETERS

Wake Model	e_{def}	W_{def}
Equilibrium Wake	0.675	3
Dynamic Inflow	0.35	3.5

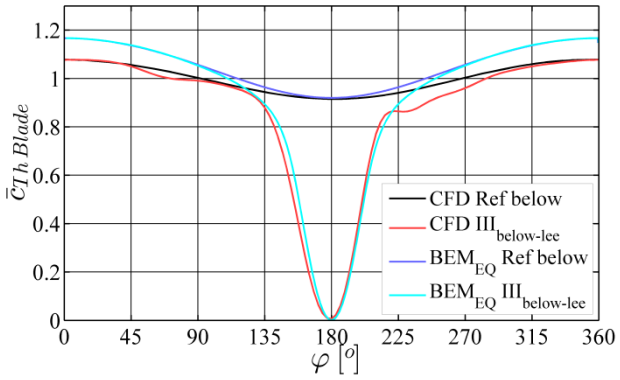

Fig. 12 relative thrust coefficient $\bar{c}_{Th\,Blade}$ of CFD and BEM with Equilibrium Wake model for operation below rated

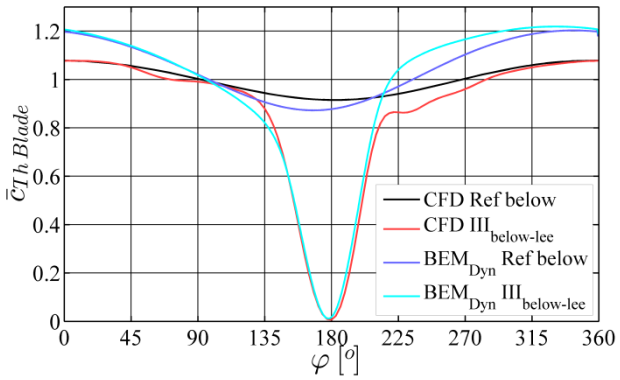

Fig. 13 relative thrust coefficient $\bar{c}_{Th\,Blade}$ of CFD and BEM with Dynamic Inflow model for operation below rated

V. Conclusions

In this research the interaction of rotor and foundation and its influence on thrust and power coefficients of a TEC has been investigated. It has been shown, that multiple vortex structures exist, which have an influence to the rotor blade hydrodynamics and loads. Also has been shown that BEM compares well to CFD in global coefficients for the analyzed load case simulations if appropriate parameters are used.

VI. Acknowledgment

This research has been conducted within a joint project of Stuttgart Wind Energy, University Stuttgart, and Voith Hydro Ocean Current Technologies GmbH & Co. KG.

VII. References

[1] S. Alscher, F. Biskup „Validierung der strömungsmechanischen Simulation eines Gezeitenströmungsrotors mit experimentellen Modellversuchen“, thesis, University Stuttgart, Germany, Jan. 2011
[2] M. Arnold, F. Biskup, D. Matha „Untersuchung einer Gezeiten-strömungsturbine und Haltestruktur mittels strömungsmechanischer Simulation“, thesis, University Stuttgart, Germany, Okt. 2011
[3] F. Biskup, P. Daus, R. Arlitt „Auslegung und Evaluierung eines Rotordesigns für Gezeitenströmungsanlagen“ in 34. Dresdner Wasserbaukolloquim, 2011
[4] CFX Theory Guide, Ansys, 2013
[5] (2013) The EMEC website. [Online]. Available: www.emec.org.uk/

[6] R. Gasch, J. Twele „Windkraftanlagen - Grundlagen, Entwurf, Planung und Betrieb“, 5th Edition, Stuttgart, Germany: Teubner-Verlag, 2007
[7] A. v. Müller, P. Daus, P. Schwarz, P. Jeschke „Characterization of the Turbulent Flow Field at a Site for Tidal Turbine Installation Based on Acoustic Doppler Current Profiler Measurements“, thesis, Rheinisch-Westfälische Technische Hochschule Aachen, Germany, Apr. 2011
[8] A. Pang, M. Skote, S. Lim „Turbulence Modeling Around Extremly Large Cylindrical Bluff Bodies“ International Offshore and Polar Engineering Conference, 2013
[9] D. Pitt, D. Peters „Theoretical Prediction of Dynamic-Inflow Derivatives“, Vertica., Vol. 5, pp. 35-53, 1981
[10] H. Snel, J.G. Schepers „Engineering moles for dynamic inflow phenomena“, Journal of Wind Engineering and Industrial Aerodynamics, Vol. 39, pp. 267-281, 1992
[11] Tidal Bladed Theory Manual, Garrad Hassan, 2012
[12] (2013) The Voith website. [Online]. Available: http://www.voith.com